RSC Advances

PAPER

View Article Online
View Journal | View Issue

Cite this: *RSC Adv.*, 2023, **13**, 873

Large-scale production of polyimide micropore-based flow cells for detecting nano-sized particles in fluids

Mostafa Salehirozveh, [ac] Alessandro Porro[bc] and Federico Thei *[c]

In diagnostic and sequencing applications, solid-state nanopores hold significant promise as a single-molecule sensing platform. The fabrication of precisely sized pores has traditionally been challenging, laborious, expensive, and inefficient, which has limited its applications until recently. To overcome this problem, this paper proposes a novel, reliable, cost-effective, portable, mass-productive, robust, and ease-of-use micropore flow cell that works based on the resistive pulse sensor (RPS) technique in order to distinguish the different sizes of c nanoparticles. RPS is a robust and informative technique that can provide valuable details of the size, shape, charge, and individual particle concentrations in the media. By femtosecond laser drilling of a polyimide substrate as an alternate material, translocation of 100, 300, and 350 nm polystyrene nanoparticles in PBS buffer was distinguished by 0.1, 1, and 2 nA current blockade levels, respectively. This is the first time a micropore has been opened in a polyimide membrane using a femtosecond laser in a single step. The experimental and theoretical investigation, scanning electron microscopy and focused ion beam spectroscopy were performed to comprehensively explain the micropore's performance. We showed that our innovative micropore-based flow cell could distinguish nano-sized particles in fluids, and it can be used in large-scale production because of its simplicity and cost-effectiveness.

Received 22nd November 2022
Accepted 12th December 2022

DOI: 10.1039/d2ra07423k

rsc.li/rsc-advances

1. Introduction

Recent scientific interest in nanopore-based detection has been sparked by its ability to detect nano-sized particles and biomolecules in media without labelling.[1] Nanopores can be formed by a protein, or they can be drilled as a hole in synthetic materials such as silicon, graphene, or polymers. The presence of a nanopore in an electrically insulating membrane can serve as a single-entity detector. There are various pores in a membrane, including biological protein channels in high electrical resistance lipid bilayers, solid-state pores, and hybrids of both membranes.[2,3] Nanopore analysis is a simple approach by inferring information about a molecule's size, shape, charge, and dipole based on the blockages in ionic current caused by molecules passing through the pore.[4,5] An ionic current is monitored through the nanopore as a voltage is applied across the membrane. Nano-size particles or molecules like DNA or proteins passing through the nanopore affect the current level, leading to a translocation event signal.[5] In other words, the method is an intrinsically single molecule, allowing the precise measurement of individual particles in real-time without the bias induced by signal amplification and alleviating most of the uncertainty associated with ensemble analysis.

In light of remarkable advances of nanopores in particle detection based on their size, a significant amount of effort has been put into improving solid-state nanopores' sensing performance to achieve high and standard levels of reproducibility and sensitivity comparable to protein pores due to their robustness and stability under tough conditions (such as temperature, electric field, and pH), and capability of integration into embedded electronics and systems. Nanopore detection generally works by placing an isolating membrane between two electrolyte-filled compartments and connecting them only by a nanoscale aperture. An insulating membrane with dimensions comparable to those of a molecule of interest is used to drive ionic current through a tiny hole. An abrupt current decrease is observed during particle/molecule translocation through each pore, known as a resistive pulse.[6,7] Nowadays, resistive pulse sensors (RPS) have gained considerable attention because of their ability to read particles by particle, have high sensitivity, and provide a wealth of information about particles contained in a suspension, such as shapes, dimensions, charges, and particle concentrations.[8–11] An electrical field funnel-shaped is generated when a voltage is applied between the two chambers.[12] The sign of a particle's charge determines whether it is driven toward or away from a nanopore. Injecting polystyrene (PS) nanoparticles into the

[a]Department Of Physics And Astronomy, University of Bologna, Bologna, Italy
[b]Department of Biosciences, University of Milan, Milan, Italy
[c]Elements SRL, Cesena, Italy. E-mail: fthei@elements-ic.com

Cis chamber and applying a negative voltage force them to translocate through the chamber since they are negatively charged at pH 7.5.[13,14]

Furthermore, it is possible to determine the electro-kinetic acceleration of nanoparticles by their translocation times based on their stimulus voltage and nanopore length. As faster translocations imply greater surface charges of the nanoparticle, the zeta potential of the particle is measured as the slope of translocation time with voltage.[6,15–17] Nanoparticles are particularly useful for the detection of biomolecules such as DNA,[18–21] proteins,[22–25] and viruses[26,27] by solid-state nanopores. Functionalized nanoparticles with target-specific receptors will change in size when bound to targets. Herein, a current blockade difference will be seen when they translocate through nanopores than non-reacted nanoparticles. The approximate of a particular species in a matrix and real/clinical samples containing different biomolecules can be estimated by counting spikes with higher amplitude (particles bound to target molecules) in contrast to small peaks (not reacted nanoparticles). The RPS is a well-developed technology used to detect particles in the fluid and measure their sizes. By the grace of the RPS technique, a relatively high number of targets in aqueous solutions can identify accurately, quickly, and reliably.[28–31]

Nanopores can be designed geometrically and mechanically to achieve high selectivity and sensitivity by mechanical and chemical modification.[32,33] Solid-state nanopore fabrication by drilling into thin membranes in a vacuum or using a transmission electron microscope (TEM) has been hampered until recently by the difficulty and expense.[34] During these laborious, time-consuming processes, only a small percentage of pores are suitable for single-molecule sensing, and extensive training and facilities are required.

Many researchers have also been interested in alternative materials that minimize fabrication steps, like using a quartz capillary with a nanoscale tip for DNA detection or polymeric membranes with the aid of an etching technique, which eliminates the need for cleanroom nanofabrication and semiconductor processing technologies.[35–37] Polymer membranes typically consist of Polyethylene terephthalate (PET) or polyimide film (PI). However, the high thermal stability, chemical resistance, mechanical and electrical properties, as well as the high resistance and breakdown voltage of PI, make it a better choice than PET.[38,39] On the other hand, PI insulating properties make it an attractive candidate for decreasing device capacitance-induced current noise.[40] Nevertheless, due to their micron-scale thickness, it is difficult to detect current modulations in common PI membranes such as Kapton films. Finding innovative materials and processes that can decrease production times whilst cost-effective and improving signal quality is imperative. To address this bottleneck, we fabricated an innovative micropore-based flow cell to distinguish nano-sized particles in fluids that is portable, sensitive, and fast in nano-sized particle detection. It can be used in large-scale production because of its simplicity and cost-effectiveness. Our portable platform utilizes a USB-powered patch clamp amplifier to record measurements, which is 101 × 44 × 18 mm in size and made from PMMA and PI, the low-cost and most abundant polymers,[41–43] as well as drilling with a femtosecond laser machine, which requires no consumables. The speed is less than a fraction of a second; consequently, this method is economical for mass production.

In the past two decades, nanopores have been discovered as an effective and reliable tool for counting molecules.[44,45] Our goal was to find alternate materials and processes to shorten production times while lowering costs and improving signal quality. We were able to fabricate micropores in a single step, which is the first time a micropore has been opened in a PI membrane using a femtosecond laser. The design and fabrication methods have been intended to be easily transferred to a large scale.

2. Material and method

2.1. Material

PI (PI) film was purchased from SHENGYI TECHNOLOGY CO., LTD. Three different sizes of polystyrene particles were purchased from Sigma-Aldrich. All chemicals were purchased from Sigma-Aldrich and used without further purification. Focus ion beam (FIB) and scanning electron microscopy (SEM) images were taken at the CNR (Consiglio Nazionale delle Ricerche) of Modena.

2.2. The flow cell design and structure

The flow cell frame consists of two elements made in PMMA that exhibit unique mechanical and electrical insulator properties in dry conditions and is almost water-resistant (Fig. 1a and c).[46] It is assumed to consider a significant increase in the ionic current due to buffer leakage, which was not observed in this experiment. The bottom and top compartments of the flow cell have designed cavities with specific characteristics, including a 4 mm diameter hole in the top part with a thickness of 5 mm and an arc-shaped cavity with 0.8 mm deep in the bottom element with a thickness of 1.6 mm. Fabricated silver electrodes were mounted on each side of the 12.6 μm thick PI film (Fig. 1b). To complete the flow cell structure, the PI film is placed between the two PMMA elements and fixed by a solvent-

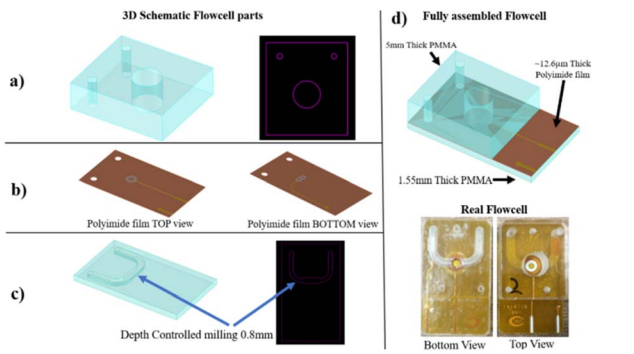

Fig. 1 Stack schematics view and real images of the flow cell. Schematic representation of (a) top PMMA element, (b) PI film including the two Ag electrodes, and (c) bottom PMMA element. (d) The schematic and real images of the fully assembled flow cell.

resistant glue to prevent liquid leakage between the layers (Fig. 1d). To allow the injection of fluids in the bottom compartment, two small through holes are drilled in both the top PMMA element and the PI film (Fig. 1a and c). Once the flow cell is assembled, the two compartments are washed with 10% v/v ethanol/water to remove dust and contaminants prior to the laser drilling process.

2.3. The drilling of single-micropore membranes

The Ag wires were mounted on PI film as electrodes in order to apply a voltage across the micropore by Kirana company. Then, the mounted PI film was placed between two PMMA compartments of the flow cell and drilled by a femtosecond laser. Finally, to make quasi-reference electrodes, silver wires were chlorinated by filling the flow cell with diluted NaOCl.

2.4. Resistive pulse sensor (RPS) analysis

After assembling the micropore flow cell, the chamber was filled with PBS × 1 at pH 7.4, and the 400 mV potential was applied to the silver wires to observe the current. The data were recorded by Elements SRL nanopore reader using 50 kHz and a 5 kHz low-pass filter. This study analysed the ionic current levels using Elements Srl's software, which can be downloaded from **https://elements-ic.com/edr_setup**.

3. Results and discussion

3.1. PI micropores characteristics

A femtosecond UV laser is used to drill the PI film to create the micropore with high accuracy in shape and size. The pores in a conical shape were prepared as part of the sensor preparation. As a result, the effective length of the asymmetric pore is shorter since the pore's resistance is located at the micropore's tip. The smaller resistance of a conical micropore is also responsible for resulting higher level of current at the same voltage as a cylindrical pore.[47–50] The ion current signal contains information about the translocation events, the chemical properties, and the sensed biomolecule's structural characteristics. As large molecules translocate the pore, the signal's amplitude is reduced. Regardless of whether the molecule is dissolved in a buffer or not, the current signal needs to be stable. A current fluctuation behavior has also been observed in the polymeric micropore. However, polyethylene terephthalate (PET) conical pores have fluctuated the current that can reach 100% of the signal when a constant voltage is applied.[19–22] PI nanopores display very stable electrical currents over different electrolytes and pHs. PI was used to create micropores because of its higher mechanical properties, greater thermal stability, and superior insulating properties *versus* other polymers.[52,53]

This section describes a single conical micropore drilled by a femtosecond laser in a PI substrate. Here, a single 1 μm pore with a length of 12.6 μm was drilled by femtosecond laser, which is significantly larger than the previous reports on solid-state nanopores. Because the large aspect ratio effectively provides a higher temporal resolution, the observations of long-term translocations are thought to be attributed to it.

A series of conical PI micropores were prepared and studied. Drill hole precision and smoothness are affected by substrate materials and laser radiation. An SEM image of a drilled 1 μm tip opening hole in a PI membrane with a 9.5 μm base opening hole is shown in Fig. 2a. A focused ion beam (FIB) cross-section

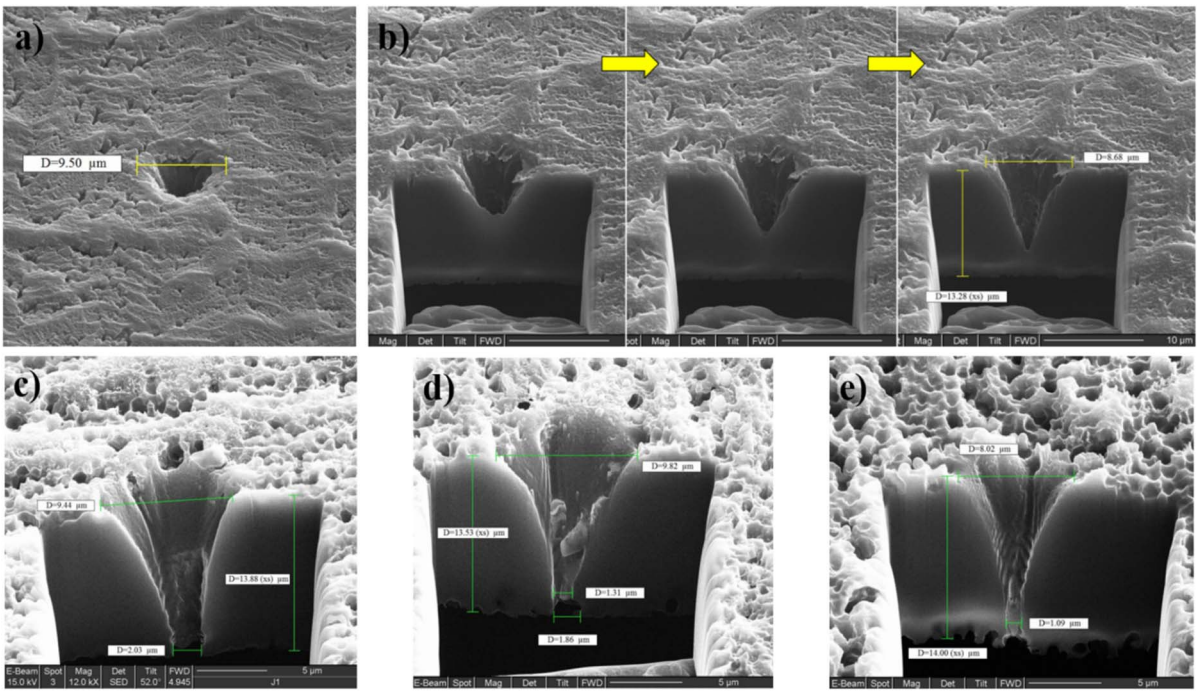

Fig. 2 (a) FIB image of single micropore in PI film drilled by femtosecond laser. (b) FIB cross-section of the hole (subsequent steps). (c, d and e) FIB cross-sections of different micropores.

subsequent steps are shown in Fig. 2b. The final images of three different individual micropores are shown in Fig. 2c–e. However, the micropore's tip diameter (narrower section) varies from around 1 to 2 μm, which is caused by the variance in the laser drilling process and parameters, even though the pore conical shape and base micropore diameter (8 to 10 μm) were similar. In addition, the PI thicknesses were approximately the same, between 13 and 14 μm. Some micropores faced problems associated with contamination or residual melted PI remaining inside the hole after laser drilling, which changed the overall shape and volume of the hole, apart from the pore diameter differences. Defected micropores did not facilitate particle translocation, resulting in fast hole clogging and particle adhesion.

Based on the diameter and shape of the hole, a micropore has a different conductance. Fig. 3 illustrates the conductance distribution of 25 micropores drilled by a femtosecond laser in PBS × 1. Some of them are not perforated, but the average values indicate that the 2 μm pore has one micro siemens (1 μS) conductance. The micropore's diameter varied over the range of 1000 to 2200 nm with a big opening of 4 to 7 μm. Also, 24% of PI films were not drilled after lasering. During the drilling process, the PI may squeeze out of the laser's confocal point, resulting in incorrect drilling. The conductance of about 1 μS and 710 nS correspond to pores having a size of about 2 μm and 1 μm, respectively.

After mounting the Ag wires on PI film, to make quasi-reference electrodes, silver wires were chlorinated. As a result of presenting NaOCl into the chambers in contact with PI to chlorinate the electrodes, the micropore hydrophilicity and conductance were affected (Fig. 4). Following immersion in NaOCl for 2.5 min, Fig. 4 shows a 50% change in the hydrophobicity of PI film. Fig. 5a and b show the electrode chlorination effect on *I–V* curves in PBS × 1 and pH 7.4 of micropores after 2.5 and 5 min chlorination by NaOCl 50% solution, respectively. As shown in Fig. 5a, the diameter of the micropores expanded when chlorination time exceeded 2.5 min.

3.2. Polystyrene NP translocations through PI micropores

By electrostatic interaction, gold nanoparticles (GNPs) with opposite surface charges can form aggregates, so the translocation of GNPs alone is difficult.[54,55] For this reason, PS nanoparticles with 100, 300, and 350 nm diameters were used to study the performance of the device in differentiation of the particles based on their size by analysing the translocation peaks of each particle.

In the context of the medium with resistivity, ρ, the pore diameter, d_p, pore length, l_p, the volume of the nanoparticle, Λ, and the shape and the orientation angle-dependent electrical shape factor, γ, the current blockade's amplitude can estimate by the following equation[51,56]

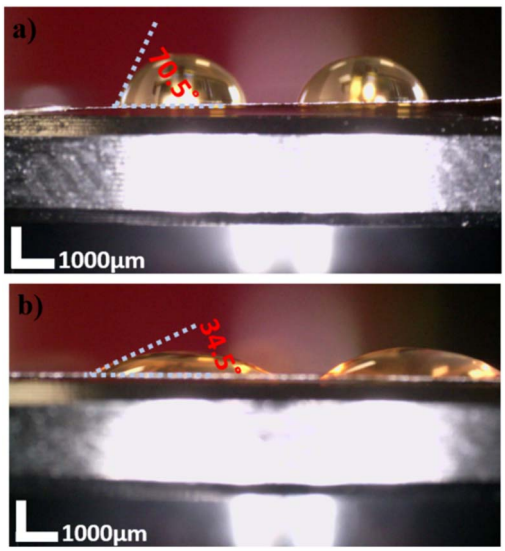

Fig. 4 Contact angle measurement of the bare PI membrane (a) and NaOCl treated for 2.5 minutes (b). The scale bar marks 1000 μm.

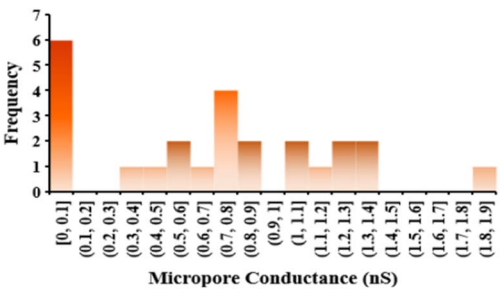

Fig. 3 Conductance distribution of 25 micropores drilled by a femtosecond laser.

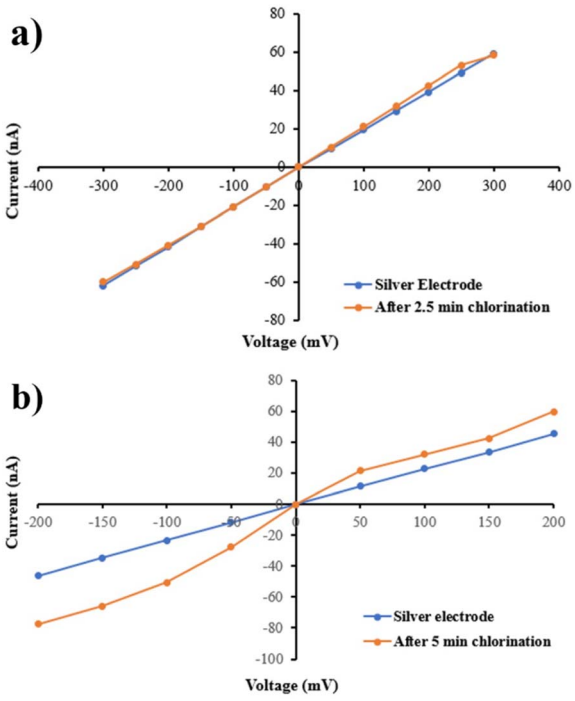

Fig. 5 *I–V* curves for PI micropore after 2.5 min (a) and 5 min (b) chlorination by NaOCl in PBS × 1 and buffered at pH 7.4.

$$\frac{\Delta I}{I_0} = \frac{4\Upsilon\Lambda}{\pi {d_p}^2\left(I_p + \frac{\pi}{4}d_p\right)} \quad (1)$$

I_0 is the current passes of the micropore in the absence of particles, and ΔI is the magnitude of the current change caused by nanoparticles passing through the nanopore. A full sphere has a Υ of 1.5. Particles are translocated according to their volume, and $\Delta I/I_0$ is the normalized magnitude of the resistive pulse.

Micropores should be small enough to detect the smallest particles and large enough to prevent clogging and particle interaction with their side walls. A biomolecule is normally detected by the immobilization of receptors such as DNA aptamers, antibodies, and enzymes on nanoparticles or the inner walls of nanopores. The most common receptor length is between 2 to 12 nm.[57] Functionalized 100 nm PS particles could be approximately 120 nm in diameter when receptors are immobilized on their surface, and particles fully covered with viruses could be approximately 300 nm. So, 12.985 μm of l_{eff} based on 12.2 μm PI thickness and 1 μm d_p were used. Therefore, the calculated current blockade level for 100 and 300 nm PS particle translocation was 0.0007 × I_0 0.0295 × I_0, respectively.

This microwell was filled with PBS × 1 and buffered at pH 7.4. A 400 mV voltage was applied as an electric field across the micropore, resulting in a baseline current of 100 nA. Then, 2 × 10^9 NPs per mL PS was added to the tip side of the pore (Cis chamber) to detect.

Fig. 6 shows significantly fewer translocations when PS was added to the micropore's base side, possibly due to molecule entanglement in the narrowing taper. As illustrated in Fig. 6, a current trace was recorded while 300 nm PS was present at ±400 mV. Several blockade events were observed for up to 1% of the baseline current signal level (~1 nA). Observation of these events correlates with the passage of PS particles through the micropore. Only three 300 nm PS nanoparticles can simultaneously translocate from a micropore with a size of 1 μm.

The PI pore provides a stable current signal easily sampled at 50 kHz and a 5 kHz low-pass filter. As a result of the high sampling rate, the translocation event of different PS sizes can be compared based on time and amplitude. Fig. 7a shows a fragment of a 10 second recording of 100, 300, and 350 nm PS nanoparticles when 400 mV voltage was applied. Scatter plots of blockade events for PS nanoparticles of different sizes are shown in Fig. 7b. By increasing the size of the PS particle, the number of transactions at the same voltage has increased. The dwell translocation events were not significantly affected by changing the size of the PS nanoparticle. PS nanoparticles with a diameter of 350 nm exhibited a shorter dwell time than those with 100 nm dimensions. However, the dwell time increased slightly when the PS nanoparticles' size increased from 100 to 300 nm. As expected, the amplitude has also increased. The current blockade for 100 and 300 nm is around 0.1 nA and 2.2

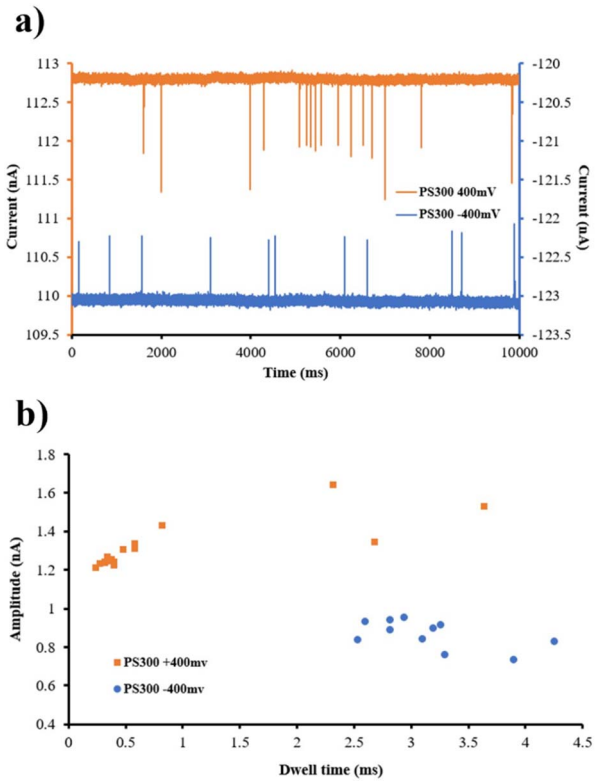

Fig. 6 300 nm PS nanoparticle translocations through a PI micropore (a) and dwell time *vs.* conductance blockade scatter plot for 300 nm PS nanoparticles (b) in +400 mV and −400 mV stimulus voltages.

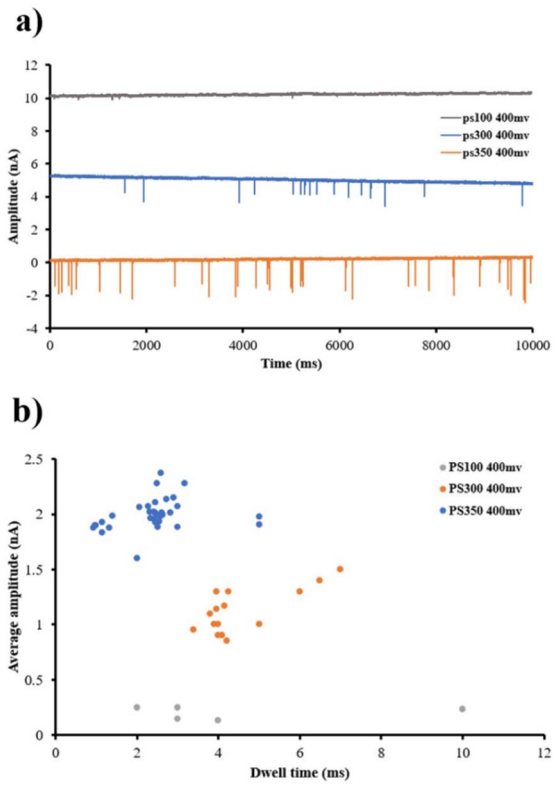

Fig. 7 Various PS nanoparticle sizes translocations through a PI hole (a). Dwell time *vs.* conductance blockade scatter plot of 100, 300, and 350 nm PS nanoparticles (b).

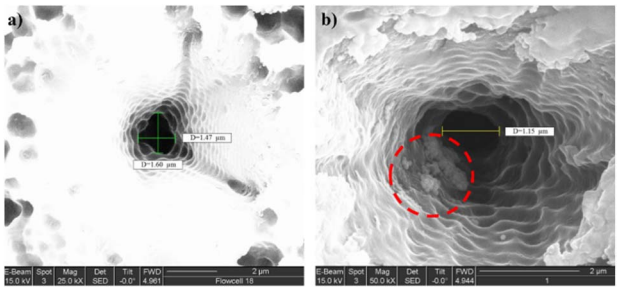

Fig. 8 Focused ion beam images of the sidewall of micropore (a) before translocation and (b) after 100 nm PS particle translocations. The 100 nm PS particles stuck to the micropore side-wall after translocation are highlighted in a red circle.

nA, respectively. These values are close to the estimated current blockade for 100 and 300 nm PS particles, around 0.07 nA and 3 nA (I_0 = 110 nA), respectively. The little difference between experienced and estimated ΔI comes from various factors, including the conical shape of the micropore in this work instead of the cylindrical shape, the non-uniform thickness of PI film, the orientation of the particles, sticking of the particles to each other or pore side-wall, and size distribution of PS particles.

Fig. 8 shows the top-view image of the micropores before and after 100 nm PS translocation. By paying attention to the pore wall image shown in Fig. 8b, agglomerated particles can be seen, which are stuck to the micropore walls, probably due to sedimentation and drying after the experiments.

4. Conclusion

A feasibility study was conducted on laser drilling of the PI films for biomolecular sensing. Handling and transferring the films between laboratories was feasible. The shape and diameter of the micropore are adaptable. In this study, a precise created 1 μm pore in PI film could detect different sizes of PS nanoparticles. A micropore flow cell made of PI membrane and PMMA chamber with one-micrometer holes can distinguish particles with 100, 200, 300, and 350 nm diameters. The thickness of the PI micropore was 12.6 μm, which resulted in a short effective length for one micropore diameter. As a result, the value of the current blockade was different by passing the variety size of PS particles through the micropore. The 1 μm pore could distinguish 100 nm from 300 nm PS nanoparticles in this work by changing the electrical resistance. Therefore, this micropore fellow cell has the potential to differentiate between bare PS and modified one with viruses.

PI micropores, owing to their chemical and physical stability, provide great flexibility in evaluating the translocation of polynucleotides under different conditions, like changing buffers or temperature. One of the benefits of using PI layers for creating micropores is the ability to modify and control their surfaces chemically. This research suggests that micropores in PI film provide the basis for developing viruses-specific sensors, and this method can be a promising technique for coronavirus detection.

Conflicts of interest

There are no conflicts of interest to declare.

Acknowledgements

This project has received funding from the Marie Skłodowska-Curie MSCA-ITN Single-Entity Nanoelectrochemistry, Sentinel [812398].

References

1 F. Dogan Guzel and H. Avci, Fabrication of Nanopores in an Ultra-Thin PI Membrane for Biomolecule Sensing, *IEEE Sens. J.*, 2018, **18**, 2641–2646.
2 J. Li, D. Stein, C. McMullan, D. Branton, M. J. Aziz and J. A. Golovchenko, Ion-beam sculpting at nanometre length scales, *Nature*, 2001, **412**, 166–169.
3 J. J. Kasianowicz, E. Brandin, D. Branton and D. W. Deamer, Characterization of individual polynucleotide molecules using a membrane channel, *Proc. Natl. Acad. Sci. U. S. A.*, 1996, **93**, 13770–13773.
4 E. C. Yusko, B. R. Bruhn, O. M. Eggenberger, *et al.*, Real-time shape approximation and fingerprinting of single proteins using a nanopore, *Nat. Nanotechnol.*, 2016, **12**, 360–367.
5 K. Briggs, H. Kwok and V. Tabard-Cossa, Automated Fabrication of 2-nm Solid-State Nanopores for Nucleic Acid Analysis, *Small*, 2014, **10**, 2077–2086.
6 E. L. C. J. Blundell, R. Vogel and M. Platt, Determination of Zeta Potential via Nanoparticle Translocation Velocities through a Tunable Nanopore: Using DNA-modified Particles as an Example, *JoVE*, 2016, **2016**, e54577.
7 L. Yang and T. Yamamoto, Quantification of virus particles using nanopore-based resistive-pulse sensing techniques, *Front. Microbiol.*, 2016, **7**, 1500.
8 E. L. C. J. Blundell, L. J. Mayne, E. R. Billinge and M. Platt, Emergence of tunable resistive pulse sensing as a biosensor, *Anal. Methods*, 2015, **7**, 7055–7066.
9 Y. Song, H. Zhang, and M. Li. Microfluidic Resistive Pulse Sensor. in *Encyclopedia of Microfluidics and Nanofluidics* 2015; pp. 1993–2000.
10 T. Vaclavek, J. Prikryl and F. Foret, Resistive pulse sensing as particle counting and sizing method in microfluidic systems: Designs and applications review, *J. Sep. Sci.*, 2019, **42**, 445–457.
11 E. Weatherall, P. Hauer, R. Vogel and G. R. Willmott, Pulse Size Distributions in Tunable Resistive Pulse Sensing, *Anal. Chem.*, 2016, **88**, 8648–8656.
12 A. Fuliński, I. Kosińska and Z. Siwy, Transport properties of nanopores in electrolyte solutions: the diffusional model and surface currents, *New J. Phys.*, 2005, **7**, 132.
13 M. Chinappi, M. Yamaji, R. Kawano and F. Cecconi, Analytical model for particle capture in nanopores elucidates competition among electrophoresis, electroosmosis, and dielectrophoresis, *ACS Nano*, 2020, **14**, 15816–15828.

14 L. Shi, X. He, J. Ge, T. Zhou, T. Li and S. W. Joo, The Influence of Electric Field Intensity and Particle Length on the Electrokinetic Transport of Cylindrical Particles Passing through Nanopore, *Micromachines*, 2020, **11**, 722.
15 T. Ito, L. Sun and R. M. Crooks, Simultaneous determination of the size and surface charge of individual nanoparticles using a carbon nanotube-based coulter counter, *Anal. Chem.*, 2003, **75**, 2399–2406.
16 D. Kozak, W. Anderson, R. Vogel, S. Chen, F. Antaw and M. Trau, Simultaneous size and ζ-potential measurements of individual nanoparticles in dispersion using size-tunable pore sensors, *ACS Nano*, 2012, **6**, 6990–6997.
17 Y. Qiu, C. Yang, P. Hinkle, I. v. Vlassiouk and Z. S. Siwy, Anomalous Mobility of Highly Charged Particles in Pores, *Anal. Chem.*, 2015, **87**, 8517–8523.
18 A. Karmi, H. Dachlika, G. P. Sakala, D. Rotem, M. Reches and D. Porath, Detection of Au Nanoparticles Using Peptide-Modified Si3N4Nanopores, *ACS Appl. Nano Mater.*, 2021, **4**, 1000–1008.
19 L. Z. Wu, Y. Ye, Z. X. Wang, *et al.*, Sensitive Detection of Single-Nucleotide Polymorphisms by Solid Nanopores Integrated With DNA Probed Nanoparticles, *Front. Bioeng. Biotechnol.*, 2021, **9**, 502.
20 R. Akahori, K. Esashika, I. Yanagi and T. Saiki, Target DNA detection by solid-state nanopores using gold nanoparticle probes, *Jpn. J. Appl. Phys.*, 2020, **59**, 107001.
21 Y. Zhang, X. Chen, C. Wang, H. C. Chang and X. Guan, Nanoparticle-assisted detection of nucleic acids in a polymeric nanopore with a large pore size, *Biosens. Bioelectron.*, 2022, **196**, 113697.
22 K. Chuah, Y. Wu, S. R. C. Vivekchand, *et al.*, Nanopore blockade sensors for ultrasensitive detection of proteins in complex biological samples, *Nat. Commun.*, 2019, **10**, 1–9.
23 R. Ren, M. Sun, P. Goel, *et al.*, Single-Molecule Binding Assay Using Nanopores and Dimeric NP Conjugates, *Adv. Mater.*, 2021, **33**, 2103067.
24 X. Lin, A. P. Ivanov and J. B. Edel, Selective single molecule nanopore sensing of proteins using DNA aptamer-functionalised gold nanoparticles, *Chem. Sci.*, 2017, **8**, 3905–3912.
25 Q. Li, Y. L. Ying, S. C. Liu, Y. Lin and Y. T. Long, Detection of Single Proteins with a General Nanopore Sensor, *ACS Sens.*, 2019, **4**, 1185–1189.
26 C. Horejs, Artificially intelligent nanopore for rapid SARS-CoV-2 testing, *Nat. Rev. Mater.*, 2021, **6**(8), 650.
27 L. Chazot-Franguiadakis, J. Eid, M. Socol, *et al.*, Optical Quantification by Nanopores of Viruses, Extracellular Vesicles, and Nanoparticles, *Nano Lett.*, 2022, **22**(9), 3651–3658.
28 Z. Tang, G. Choi, R. Nouri and W. Guan, Nanopore Digital Counting of Amplicons for Ultrasensitive Electronic DNA Detection, *Tech. Digest Int. Elect. Devices Meet.*, 2019, 18.7.1–18.7.4.
29 X. X. Li, C. Li, P. C. Du, *et al.*, Rapid and Accurate Detection of SARS Coronavirus 2 by Nanopore Amplicon Sequencing, *Front. Microbiol.*, 2022, **13**, 134.
30 M. Charron, K. Briggs, S. King, M. Waugh and V. Tabard-Cossa, Precise DNA Concentration Measurements with Nanopores by Controlled Counting, *Anal. Chem.*, 2019, **91**, 12228–12237.
31 E. L. C. J. Blundell, L. J. Mayne, E. R. Billinge and M. Platt, Emergence of tunable resistive pulse sensing as a biosensor, *Anal. Methods*, 2015, **7**, 7055–7066.
32 C. Dekker, Solid-state nanopores, *Nat. Nanotechnol.*, 2007, **2**, 209–215.
33 B. N. Miles, A. P. Ivanov, K. A. Wilson, F. Dogan, D. Japrung and J. B. Edel, Single molecule sensing with solid-state nanopores: novel materials, methods, and applications, *Chem. Soc. Rev.*, 2012, **42**, 15–28.
34 M. Y. Wu, D. Krapf, M. Zandbergen, H. Zandbergen and P. E. Batson, Formation of nanopores in a SiN/SiO2 membrane with an electron beam, *Appl. Phys. Lett.*, 2005, **87**, 113106.
35 L. J. Steinbock, O. Otto, C. Chimerel, J. Gornall and U. F. Keyser, Detecting DNA folding with nanocapillaries, *Nano Lett.*, 2010, **10**, 2493–2497.
36 A. Mara, Z. Siwy, C. Trautmann, J. Wan and F. Kamme, An asymmetric polymer nanopore for single molecule detection, *Nano Lett.*, 2004, **4**, 497–501.
37 C. C. Harrell, Y. Choi, L. P. Home, L. A. Baker, Z. S. Siwy and C. R. Martin, Resistive-pulse DNA detection with a conical nanopore sensor, *Langmuir*, 2006, **22**, 10837–10843.
38 K. Schmidt-Rohr, Method of producing nanostructures in membranes, and asymmetrical membrane, *Nucl. Instrum. Methods Phys. Res., Sect. B*, 2002, **280**, 536–543.
39 S. Ma, Y. Wang, C. Liu, Q. Xu and Z. Min, Preparation and characterization of nanoporous PI membrane by the template method as low-k dielectric material, *Polym. Adv. Technol.*, 2016, **27**, 414–418.
40 Y. Goto, I. Yanagi, K. Matsui, T. Yokoi and K. I. Takeda, Integrated solid-state nanopore platform for nanopore fabrication via dielectric breakdown, DNA-speed deceleration and noise reduction, *Sci. Rep.*, 2016, **6**, 1–8.
41 L. Gammelgaard, J. M. Caridad, A. Cagliani, *et al.*, Graphene transport properties upon exposure to PMMA processing and heat treatments, *2d Mater*, 2014, **1**, 035005.
42 P. Russo, Physical Basis of x-Ray Imaging, *Comprehensive Biomedical Physics*, 2014, 1–48.
43 A. Sezer Hicyilmaz and A. Celik Bedeloglu, Applications of PI coatings: a review, *SN Appl. Sci.*, 2021, **3**, 1–22.
44 Y. He, M. Tsutsui, Y. Zhou and X. S. Miao, Solid-state nanopore systems: from materials to applications, *NPG Asia Mater.*, 2021, **13**, 1–26.
45 H. Yang, M. Saqib and R. Hao, Single-Entity Detection With TEM-Fabricated Nanopores, *Front. Chem.*, 2021, **9**, 305.
46 S. B. Aziz, O. G. Abdullah, A. M. Hussein and H. M. Ahmed, From Insulating PMMA Polymer to Conjugated Double Bond Behavior: Green Chemistry as a Novel Approach to Fabricate Small Band Gap Polymers, *Polymers*, 2017, **9**, 626.
47 L. van Oeffelen, W. van Roy, H. Idrissi, D. Charlier, L. Lagae and G. Borghs, Ion Current Rectification, Limiting and Overlimiting Conductances in Nanopores, *PLoS One*, 2015, **10**, e0124171.

48 Z. Siwy, Y. Gu, H. A. Spohr, *et al.*, Rectification and voltage gating of ion currents in a nanofabricated pore, *Europhys. Lett.*, 2002, **60**, 349.

49 J. Cervera, B. Schiedt, R. Neumann, S. Mafá and P. Ramírez, Ionic conduction, rectification, and selectivity in single conical nanopores, *J. Chem. Phys.*, 2006, **124**, 104706.

50 Z. Siwy and A. Fuliński, Origin of [Formula presented] Noise in Membrane Channel Currents, *Phys. Rev. Lett.*, 2002, **89**, 158101.

51 A. Mara, Z. Siwy, C. Trautmann, J. Wan and F. Kamme, An Asymmetric Polymer Nanopore for Single Molecule Detection, *Nano Lett.*, 2004, **4**, 497–501.

52 Z. Siwy, D. Dobrev, R. Neumann, C. Trautmann and K. Voss, Electro-responsive asymmetric nanopores in PI with stable ion-current signal, *Appl. Phys. A*, 2003, **76**, 781–785.

53 F. Dogan Guzel and H. Avci, Fabrication of Nanopores in an Ultra-Thin PI Membrane for Biomolecule Sensing, *IEEE Sens. J.*, 2018, **18**, 2641–2646.

54 Y. Yang, Y. Hu, H. Du and H. Wang, Intracellular gold nanoparticle aggregation and their potential applications in photodynamic therapy, *Chem. Commun.*, 2014, **50**, 7287–7290.

55 R. Gary, G. Carbone, G. Petriashvili, M. P. de Santo and R. Barberi, Detection of Gold Nanoparticles Aggregation Growth Induced by Nucleic Acid through Laser Scanning Confocal Microscopy, *Sensors*, 2016, **16**, 258.

56 N. Chen, M. Zhou, X. Dong, *et al.*, Epidemiological and clinical characteristics of 99 cases of 2019 novel coronavirus pneumonia in Wuhan, China: a descriptive study, *Lancet*, 2020, **395**, 507–513.

57 M. Reth, Matching cellular dimensions with molecular sizes, *Nat. Immunol.*, 2013, **14**, 765–767.